ACS APPLIED MATERIALS & INTERFACES

Research Article

www.acsami.org

Hollow $Co_{0.85}Se$ Nanowire Array on Carbon Fiber Paper for High Rate Pseudocapacitor

Abhik Banerjee,* Sumit Bhatnagar, Kush Kumar Upadhyay, Prasad Yadav, and Satishchandra Ogale*

Centre of Excellence in Solar Energy, Physical, and Materials Chemistry Division, National Chemical Laboratory (CSIR-NCL), Pune 411 008, India

Network Institute of Solar Energy (CSIR-NISE), Academy of Scientific and Innovative Research (AcSIR), New Delhi 110 025, India

Supporting Information

ABSTRACT: A supercapacitor electrode is fabricated with $Co_{0.85}Se$ hollow nanowires (HNW) array, which is synthesized by wet chemical hydrothermal selenization of initially grown cobalt hydroxyl carbonate nanowires on conductive CFP. The dense self-organized morphology of $Co_{0.85}Se$ HNWs is revealed by scanning/transmission electron microscopy. The as-synthesized $Co_{0.85}Se$ HNWs possess high pseudocapacitive property with high capacitance retention and high durability. The areal capacitance value is seen to vary from 929.5 to 600 mF cm^{-2} (60% retention) as the current density is increased from 1 to 15 mA cm^{-2}, an increase of a factor of 15. Based on mass loading, this corresponds to a very high gravimetric capacitance of 674 (for 2 mA cm^{-2} or 1.48 Ag^{-1}) and 444 Fg^{1-} (for 15 mA cm^{-2} or 11 A g^{-1}) in a full-cell configuration with the $Co_{0.85}Se$ HNWs as cathode and activated carbon as anode (asymmetric configuration) promising results are obtained.

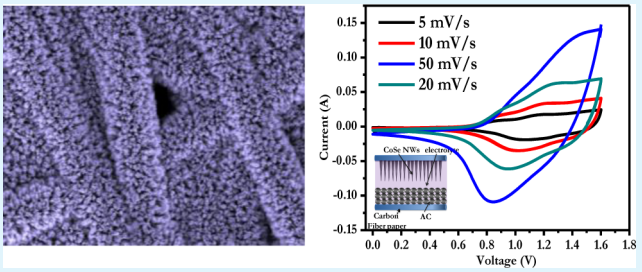

KEYWORDS: *hydrothermal, cobalt selenide, selenization, carbon fiber paper, pseudocapacitor, asymmetric supercapacitor*

1. INTRODUCTION

Energy crises due to growing populations and rapid industrial development in different parts of the world have led scientists to focus on the development of cleaner, renewable, and cost-effective energy harnessing and storage devices. Because materials are the vehicles to realize viable and efficient device designs, research on the designing and engineering of novel materials for sustainable energy is in great demand.[1−3]

Supercapacitors with large power density, faster charge−discharge, and life spans longer than those of batteries have emerged as an excellent energy storage device for a number of application sectors. Generally, two kinds of charge storage mechanisms are observed in supercapacitors. The electric double layer capacitor (EDLC) mechanism is based on ion adsorption on the surfaces by Coulombic force that mostly involves carbon-based large area conducting porous materials. On the other hand, in the case of a pseudocapacitor faradic reactions occur on the surface of the active materials.[4−6]

Transition metal oxides are strongly investigated as pseudocapacitive materials because they exhibit higher capacitance as compared to carbon, mainly because of the presence of a variety of oxidation states. Yet, the rate performance of the transition metal oxides suffers due to poor electrical conductivity.[7,8] Hence, finding a strategy for novel materials synthesis with engineered nanostructures and high conductivity is highly desired.[9] Electrode materials with higher conductivity help with the faster electron transport from the electrode material surface to the current collector, thereby decreasing the electron transfer resistance. On the other hand, proper nanostructures having large exposed electroactive surface area but low ionic diffusion resistance and shorter path length of electron diffusion are also required for high rate pseudocapacitor.[10]

Very recently, significant research effort is being expended on exploring metal sulfides for pseudocapacitive electrode.[11−14] $NiCo_2S_4$ is one such material that has a lower band gap and a higher conductivity than those of $NiCo_2O_4$ and performs much better in terms of rate capability.[15]

Similar to the interest in sulfides, very recently, there have also been a few very interesting reports on metal-selenide-based nanostructures for supercapacitor electrodes that appear quite promising.[16,17] Specifically, tin- and germanium-selenide-based 2D and 3D nanostructures have been reported; however, the corresponding capacitance values are somewhat lower than what may be desirable from the applications standpoint. This may be due to the electrochemically less active metals tin and germanium. On the other hand, transition metals have the flexibility of variety in terms of easily available (and multiple) oxidation states and therefore higher electrochemical activity than other metals. Thus, it is worthwhile to synthesize and examine electrochemically active transition metal selenides with novel nanostructures for high performance supercapacitor application. This is precisely the object of this study.

Received: July 17, 2014
Accepted: October 3, 2014
Published: October 3, 2014

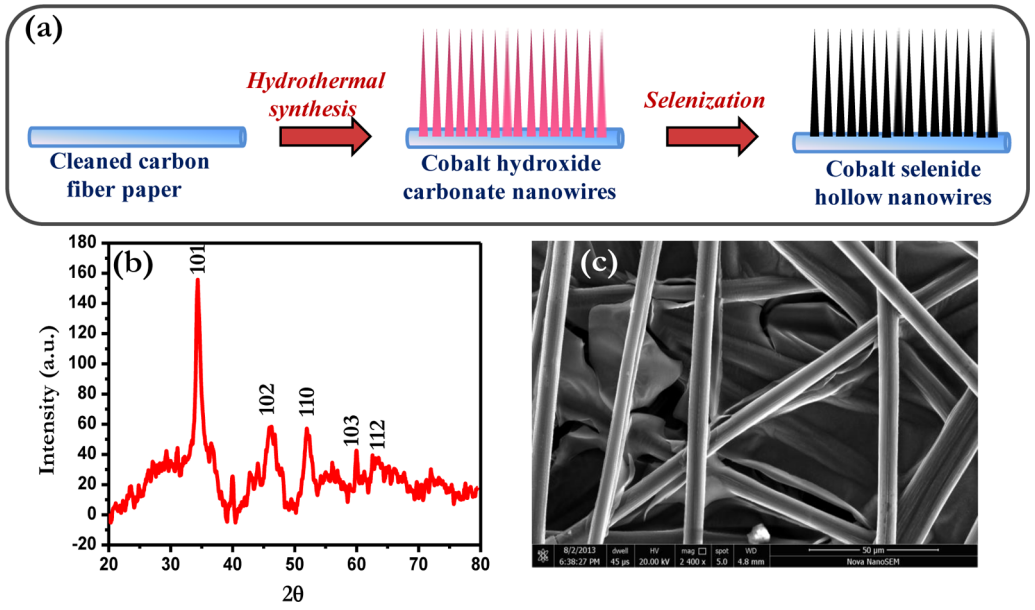

Figure 1. (a) Schematic diagram of formation of $Co_{0.85}Se$ HNWs, (b) XRD spectrum of $Co_{0.85}Se$, and (c) SEM image of the carbon fiber paper.

Among metal selenides, cobalt selenides have attracted particular attention in the energy research community because of their various superior properties. For instance, $Co_{0.85}Se$ has been successfully synthesized and used for electrocatalytic applications such as oxygen reduction and water splitting.[18,19] It has also been successfully used for the degradation of hydrazine hydrate.[18] Yet, thus far, no data has been reported on the use of cobalt-selenide-based nanostructures for charge storage applications.

In this work, we report on a novel strategy toward oriented growth of one-dimensional $Co_{0.85}Se$ hollow nanowires (HNWs) on a conductive carbon fiber paper (CFP) substrate by the Kirkendall effect. Cobalt selenide possesses a lower optical band gap and a higher conductivity than those of cobalt oxides and is thereby expected to reflect richer electrochemistry than cobalt oxides. Hollow micro/nanostructures have proved to be promising novel material forms for use in energy storage devices. Moreover, engineering hollow micro/nanostructures results in high cycling ability because the large void spaces therein facilitate the storage of a large amount of charge. Additionally, individual nanostructures synthesized by this process have a direct contact with the conductive substrate via conducting channels, thereby enhancing the electron transfer kinetics.

Of all the conductive substrates like stainless steel, nickel foam, titanium foil, graphite, carbon cloth/paper, and so on used in supercapacitor devices, CFP was chosen in this work because of its excellent characteristics of light weight, high conductivity, porosity, and chemical inertness.[20] When the electrochemical behavior of the as-synthesized CFP-supported $Co_{0.85}Se$ nanowire was investigated for supercapacitor properties using 3 M KOH solution, we found a remarkably high areal capacitance value, varying from 929.5 to 387 mF cm^{-2} (41% retention) as the current density was increased from 1 to 50 mA cm^{-2}, an increase of a factor of 50. Based on mass loading, this corresponds to a very high gravimetric capacitance of 674 Fg^{1-} (for 2 mA cm^{-2} or 1.48 Ag^{1-}) and 444 Fg^{1-} (for 15 mA cm^{-2} or 11 Ag^{1-}), which are much superior values compared to those in previous reports on selenide systems, presumably because of the distinct role of the presence of transition element in our case, as mentioned previously.[16,17] Further, in a full-cell configuration with the $Co_{0.85}Se$ HNWs as cathode and activated carbon as anode (asymmetric configuration), promising results were obtained.

2. EXPERIMENTAL SECTION

2.1. Materials. Cobalt nitrate and urea were purchased from Sigma-Aldrich, and ammonium fluoride and selenium powder were obtained from Merck. All solvents and chemicals were of reagent quality and were used without further purification.

2.2. Preparation of Carbon Fiber Paper Supported $Co_{0.85}Se$ HNWs Array. For the synthesis of initial precursor cobalt hydroxide carbonate, 10 mmol of $Co(NO_3)_2$, 20 mmol NH_4F, and 50 mmol of $CO(NH_2)_2$ were dissolved in 70 mL of distilled water to make a pink homogeneous solution, and the homogeneous solution was transferred into Teflon-lined stainless steel autoclave liners with a piece of CFP substrate immersed into the reaction solution. The autoclave was kept in the oven and maintained at 120 °C for 9 h. For the selenization process, 200 mg of sodium selenite (Na_2SeO_3) and 10 mL of hydrazine hydrate were added into the 70 mL of ethanol solution with precursor, and the mixture was kept in the autoclave at 140 °C for 12 h. Afterward, a black sample was obtained from the autoclave.

2.3. Electrochemical Measurements. Cyclic voltammetry (CV) studies, galvanostatic charge−discharge measurement and electrochemical impedance analysis were carried out using three-electrode systems (carbon-paper-supported nanowires array used as working electrode, Hg/HgO as reference electrode, and platinum strip as a counter electrode). Cyclic voltammetry was carried using 3 M aqueous KOH solution as the electrolyte at different potential scan rates (1−20 mV s^{-1}). Charging and discharging were carried out galvanostatically by varying the current density from 1 to 50 mA cm^{-2} over a potential range of 0−0.55 V. Cyclic stability was examined by galvanostatic charge−discharge at the constant current density (10 mA cm^{-2}) up to 2000 cycles.

2.4. Characterizations. Various characterization techniques such as X-ray diffraction (XRD, Philips X'Pert PRO), high-resolution transmission electron microscopy (HR-TEM, FEI Tecnai 300), and field emission scanning electron microscopy (SEM) with energy-dispersive X-ray spectroscopy (EDX) (FEI Quanta 200 3D) were used for the study.

2.5. Calculations. Areal (C_{arl}) and gravimetric specific capacitance (C_{sp}) values were calculated from charge−discharge measurement by the following equations:

dx.doi.org/10.1021/am504333z | ACS Appl. Mater. Interfaces 2014, 6, 18844−18852

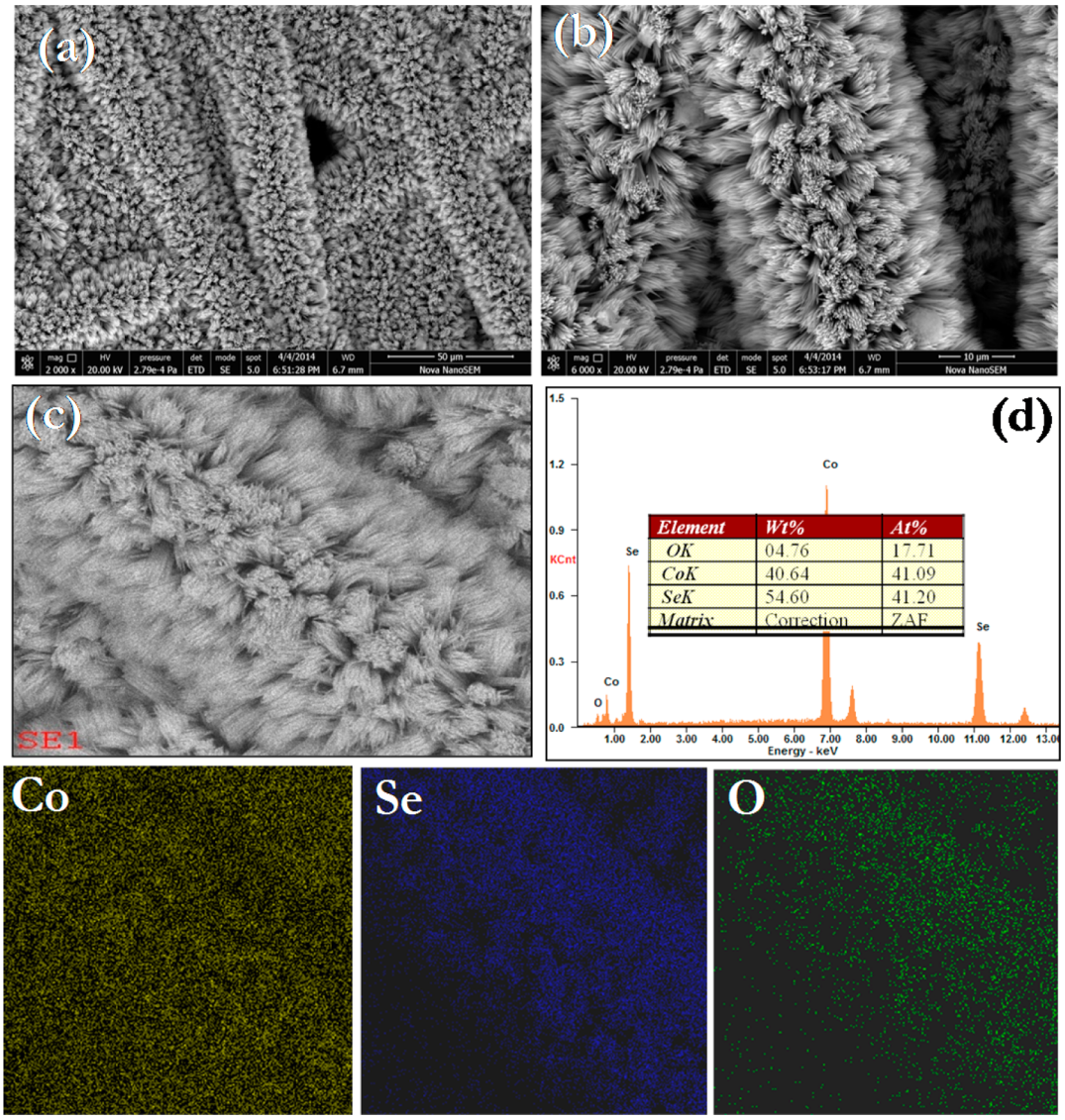

Figure 2. (a and b) SEM images of the $Co_{0.85}Se$ HNWs; (c) EDAX image and (d) its corresponding EDAX spectrum. (bottom) Elemental mappings with different color for different elements.

$$C_{sp} = \frac{I \times t}{\Delta V \times m}$$

$$C_{arl} = \frac{I \times t}{\Delta V \times s}$$

where I is the constant discharge current, t is the discharging time, ΔV is the potential window (excluding the IR drop), m is the mass of the electrode, and s is the geometrical area of the electrode.

The areal energy density (E) in Watts per square centimeter (W cm^{-2}) and power density (P) in Watts per square centimeter derived from galvanostatic charge−discharge curves are calculated from the following expression:

$$E = \frac{1}{2}C(\Delta V)^2$$

where C is the specific or areal capacitance and ΔV is the potential window.

3. RESULTS AND DISCUSSIONS

Initially, nanowires of pink cobalt hydroxide $Co_2(OH)_2(CO_3)_2$ were synthesized on conducting fiber paper by a simple hydrothermal method. Selenization of the as-synthesized $Co_2(OH)_2(CO_3)_2$ nanowires was done by adding separately prepared selenide solution followed by hydrothermal treatment. During the selenization process, the Na_2SeO_3 gets reduced to Se and further selenide ion by hydrazine hydrate, which reacts with $Co_2(OH)_2(CO_3)_2$ to form $Co_{0.85}Se$ HNWs. After selenization, the pink material changed color to dark black. A detailed experimental scheme is shown in Figure 1a. To check the phase purity of the as-synthesized samples, the XRD patterns were recorded. To perform the XRD, we scratched out CFP-supported material to avoid the very strong signal of carbon. Figure 1b shows the XRD pattern of black cobalt selenide. The corresponding peaks match with the $Co_{0.85}Se$ phase with the JCPDS data sheet no. 52-1008 (19). The peaks are marked according to their (hkl) indices, which match well with the hexagonal closed pack (HCP) arrangement. There are no other peaks corresponding to the precursor, which implies full conversion of the starting material into cobalt selenide during hydrothermal treatment.

SEM was employed to investigate the morphology and the nature of the surfaces. Figure 1c shows the SEM images of the CFP, which reveal well-connected CFP with a typical width of 5

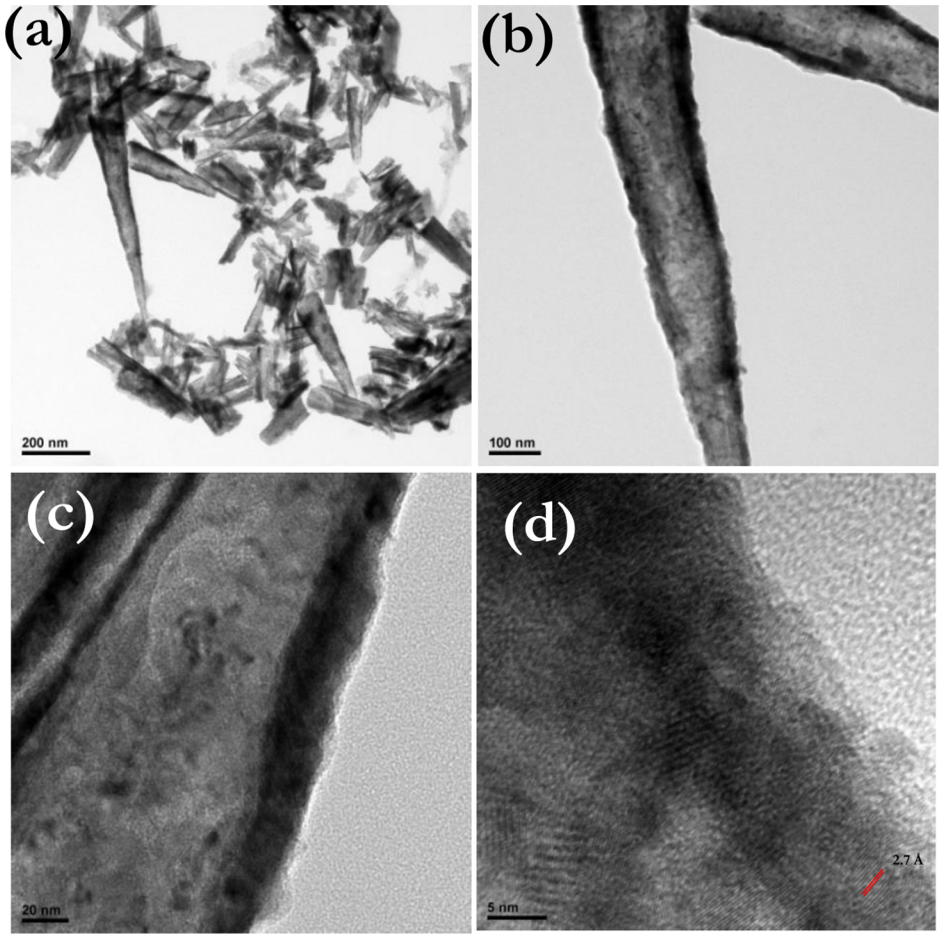

Figure 3. (a–c) TEM images and (d) HRTEM image of $Co_{0.85}Se$ HNWs.

μm. Also, the large spaces among the interconnected carbon fibers help the faster ion transport to all electroactive surfaces, which reduces the diffusion limitation for high-power supercapacitor applications. It is observed that the $Co_{0.85}Se$ nanowires are uniformly grown on the surface of the carbon fiber as seen in the SEM images (Figure 2a,b). Each nanowire is separated and individually connected with the carbon fiber which can facilitate the electronic transport as well as ion transport to the whole active area. Additionally, energy dispersive X-ray analysis (EDAX) and elemental mapping (Figure 2c,d) were done for the $Co_{0.85}Se$ nanowires. A uniform distribution of cobalt and selenium was found with their corresponding ratio of 1:1. A very low oxygen signal, which may be adsorbed moisture and oxygen on the high-surface-area sample, is also revealed.

For understanding the details of the microstructural features of the nanowires, we performed HR-TEM studies. TEM images of the $Co_{0.85}Se$ nanowires are shown in Figure 3a–c. In these, we can easily identify the tapered shaped nanowires with well-defined hollow interior. The contrast between the inside and the edge of the nanowire clearly signifies the hollow nature of the nanowire.

The formation of the hollow interior is related to the diffusion process of the cations, known as the Kirkendal effect. At the time of the selenization process, selenide ions react with the surface metal ions of cobalt hydroxide carbonate to form a thin barrier layer of cobalt selenide, which does not allow further reaction of the selenide ions with the bulk metal ions. Hence, the further reaction progresses by the diffusion of the metal ions (Co^{2+}) from bulk to surface as the dominant process over the diffusion of anions (Se^{2-}). The same effects have been observed in the case of formation of metal sulfide hollow nanostructures.[20] Here, it is important to notice that the selenization process does not change the overall morphology of the nanowire. During the high-temperature phase transformation, sometimes the structural changes happen due to Rayleigh instability.[21] This was not observed in our case because of the low-temperature selenization process. The width of the nanowires varies from 10 (close to the tip) to more than 100 nm (toward the anchoring point). Nanowires are broken due to sonication at the time of TEM sample preparation. Further HR-TEM was done at a higher magnification (up to 5 nm; Figure 3d) where lattice planes are well identified. The interplanar lattice spacing was estimated to be around 0.7 nm which closely corresponds to the (101) plane of the $Co_{0.85}Se$ phase.

To investigate the electrochemical performance of cobalt selenide, we carried out cyclic voltammetry using 3 M KOH as an electrolyte. Figure 4a shows the cyclic voltammetry data for the bare CFP electrode and the CFP-supported $Co_{0.85}Se$ nanowire forest at the scan rate of 20 mV s^{-1}. A negligible current contribution from the CFP indicates no capacitive contribution from the substrate. The nonrectangular nature of the CV curve indicates the faradic reversible reactions occur, confirming the pseudocapacitive nature of the $Co_{0.85}Se$ electrode. Two pairs of redox peaks of distinct oxidation and

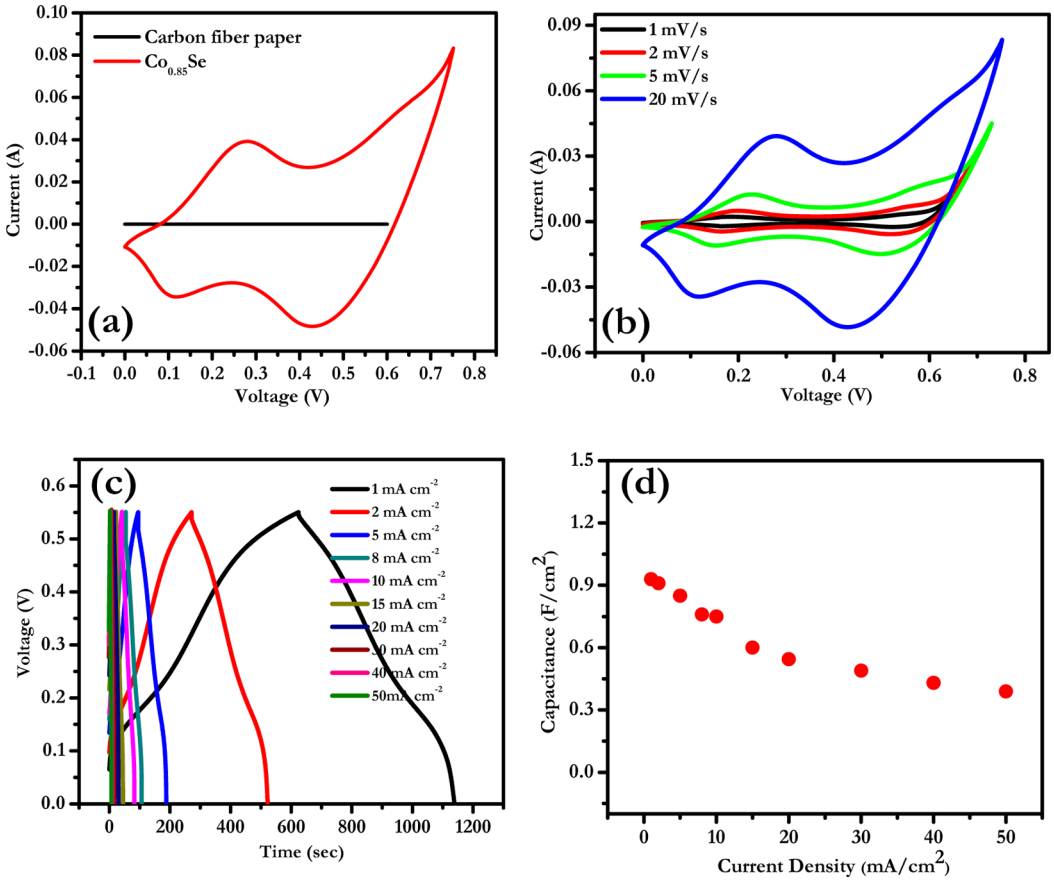

Figure 4. (a) Cyclic voltametry (CV) of the $Co_{0.85}Se$ HNWs and CFP at a scan rate of 20 mV s^{-1}; (b) the CV plot of the $Co_{0.85}Se$ HNWs at scan rated from 1 to 20 mV s^{-1}; (c) charge–discharge plots of the $Co_{0.85}Se$ at different current density values from 1 to 15 mA cm^{-2}; and (d) the capacitance of the $Co_{0.85}Se$ HNWs at different current densities.

reduction peaks is obtained from the CV of $Co_{0.85}Se$. The peaks are due to the following redox reactions:

$$Co_{0.85}Se + OH^- \leftrightarrow Co_{0.85}SeOH + e^-$$

$$Co_{0.85}SeOH + OH^- \leftrightarrow Co_{0.85}SeO + H_2O + e^-$$

Figure 4b shows the cyclic voltammetry plots at different scan rates from 1 to 20 mV s^{-1}. It is observed that with increasing scan rate, the oxidation and reduction peak current increases and the cathodic/anodic peak current shifts toward higher/lower voltage. This is associated with the Ohmic resistance, mainly because of diffusion of ions at the higher scan rate. A linear relationship between the square root of the scan rate and anodic peak current (Figure SI-1, Supporting Information) indicates good reversibility of the electrode material and confirms the faradic reaction is hydroxyl-ion diffusion-controlled.

To further evaluate the electrochemical performance of the electrode material, we performed galvanostatic charge–discharge measurement. Figure 4c shows the charge–discharge characteristics of the electrode material for the different current densities from 1 to 50 mA cm^{-2}. A deviation from linear charge–discharge curve, which is a characteristic property of EDLC, indicates pseudocapacitive nature of the as-synthesized $Co_{0.85}Se$ resulting from redox reactions by adsorption or desorption of hydroxyl ions at the electrode–electrolyte interface. The charge–discharge of as-synthesized $Co_{0.85}Se$ HNWs is extremely symmetric in nature with a coulombic efficiency of 97%, which again confirms the highly reversible nature of the electrodes. Areal capacitance was calculated, and the capacitance values were obtained as 929.5, 911.8, 847.7, 763.6, 750, 600, 545, 490, 436, and 387 mF cm^{-2} at current density values of 1, 2, 5, 8, 10, 15, 20, 30, 40, and 50 mA cm^{-2}, respectively (Figure 4d). It is very important to notice that in spite of the increase in the current density by a factor of 50, 41% of the capacitance retention takes place. This result clearly indicates the high rate performance of the electrode material, even at very high applied current densities, which is very important for practical supercapacitor applications. The capacitance values clearly reveal the advantage of any single component based electrode. These values are comparable to or higher than various reports on single material based electrochemical performance.[22−27] For instance, Luo et al. have reported single crystalline $NiCo_2O_4$ nanoneedles based electrode having a capacitance of 0.79 F cm^{-2},[22] while Kim et al. have obtained a capacitance of 0.01 F cm^{-2} for the applied current density of 0.2 mA cm^{-2}.[23] Our values are far better than those for TiO_2 nanotube film (0.911×10^{-3} F cm^{-2}) and electrodeposited MnO_2 (0.125 F cm^{-2}).[24,25] Furthermore, the areal capacitance value can be enhanced by making hybrid nanostructures with other pseudocapacitative materials.

The high conductivity of the $Co_{0.85}Se$ nanowires is the most likely reason for the high rate performance. To compare the electronic conductivity of cobalt selenide and cobalt oxide, we grew $Co_{0.85}Se$ and Co_3O_4 film on normal glass substrate. Co_3O_4 was obtained by heating the initial cobalt hydroxide carbonate precursor at 350 °C for 2 h in air. Current–voltage (I–V) plots

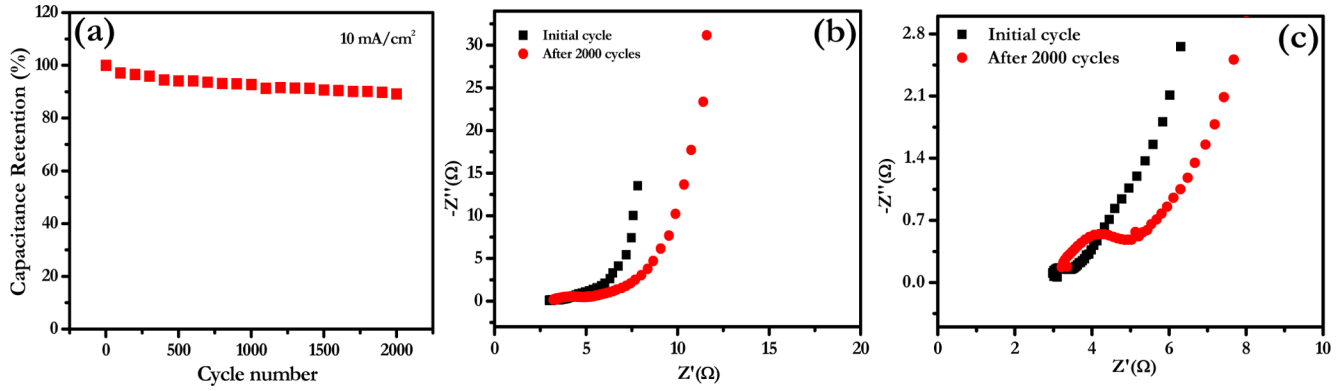

Figure 5. (a) Electrochemical cyclic stability of the $Co_{0.85}Se$ HNWS up to 2000 cycles at current density of 10 mA cm^{-2}; (b) electrochemical impedance spectra of the $Co_{0.85}Se$ HNWS; (c) magnified impedance spectra over the higher frequency region.

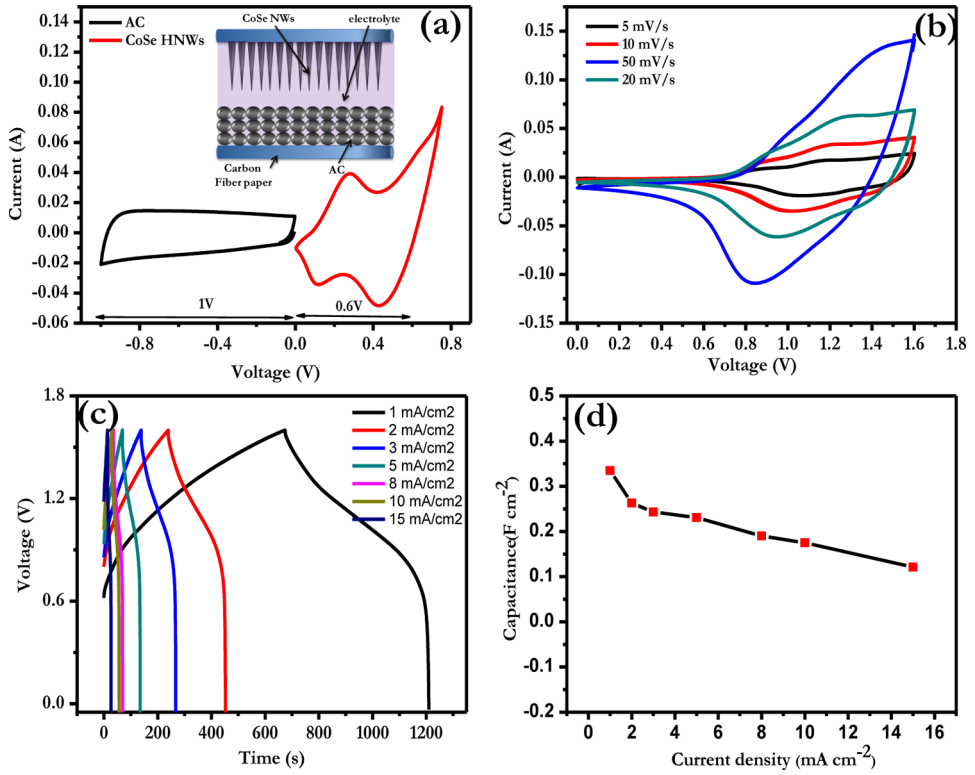

Figure 6. (a) Cyclic voltametry (CV) of the $Co_{0.85}Se$ and AC with their corresponding potential window at a scan rate of 20 mV s^{-1}; (b) CV plot of the asymmetric supercapacitor at scan rates from 5 to 20 mV s^{-1}; (c) charge−discharge plots of the asymmetric supercapacitor at different current density values from 1 to 15 mA cm^{-2}; (d) the capacitance of the asymmetric supercapacitor at different current densities.

of $Co_{0.85}Se$ and Co_3O_4 were obtained by linear sweep voltammetry (Figure SI-2, Supporting Information). A huge enhancement of current was observed in the case of $Co_{0.85}Se$ as compared to Co_3O_4. It was almost 10^9 times enhancement, which reflects the remarkably high conductivity of $Co_{0.85}Se$ hollow nanowires (HNWs) over Co_3O_4. High conductivity matters in electrochemical storage property because it helps reduce the electron spin resonance (ESR) by the faster electron transport to the current collector, thereby enhancing the high rate capability. Along with the conductivity, the hierarchal nanostructure helps by way of a quick access for electrolyte ions to the electro-active surfaces supporting the high rate performance even further.

Gravimetric capacitance was also measured according to the mass loading per square centimeter. The maximum capacitance value obtained was 688 F g^{1-} at an applied current density of 1 mA cm^{-2}. The variation of gravimetric capacitance with current density is plotted in Figure SI-3 (Supporting Information). The reported gravimetric capacitance is clearly higher than previously reported metal selenide cases (e.g., SnSe nanodiscs with a capacitance of 210 F g^{-1}[13] and $GeSe_2$-based nanostructures with 300 F g^{1-}[14] for the applied current density of 1 Ag^{-1}).

To evaluate the stability and durability of the synthesized $Co_{0.85}Se$ HNWs, cyclic stability of the material was also examined up to 2000 cycles at a high current density of 10 mA cm^{-2}; the corresponding data is shown in Figure 5a. The novel $Co_{0.85}Se$ NWs electrode shows very good long-term stability which is almost 89% of capacitance retention after cycling 2000 cycles. Lowering the capacitance value may be attributed to the

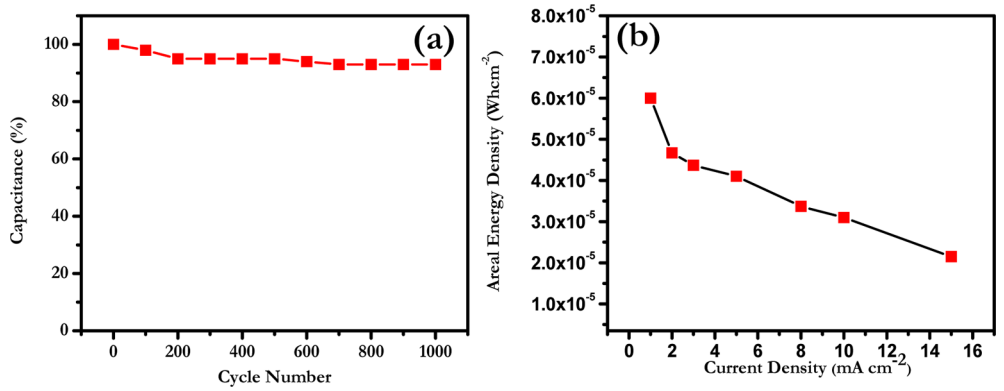

Figure 7. (a) Electrochemical cyclic stability of the asymmetric supercapacitor up to 1000 cycles at a current density of 5 mA cm^{-2}; (b) areal energy density vs different current densities from 1 to 15 mA cm^{-2}.

removal of the active material gradually with cycling. Overall, the CFP-supported $Co_{0.85}Se$ HNWs show sufficient cyclic stability at very high current density, which is important for practical applications. Thus, it is clear that the 1D $Co_{0.85}Se$ NWs array is a promising electrode material for aqueous-based supercapacitor applications in terms of high areal capacitance, rate performance, and cyclability.

As supercapacitors are the best source of power for various portable devices, low resistance of the electrode materials is electrochemically preferred for better applicability and better life cycle. Thus, in order to investigate its resistive property, we performed an electrochemical impedance spectroscopy study in the frequency range of 0.01−10^5 Hz with an amplitude of 5 mV. In general, the impedance spectra can be divided into two parts: a high-frequency region characterized by the presence of a semicircle and a low-frequency region characterized by a straight line. The high-frequency region is particularly important because it can be used to characterize the material properties such as equivalent series resistance (sum of the contact resistance, electrolyte resistance, and material resistance) from the intercept of the semicircle on the real axis. The charge transfer resistance, R_{ct}, can be obtained from the diameter of the semicircle.

Figure 5b shows the Nyquist plots for the cobalt selenide case for initial cycle and after 2000 cycles. A longer Warburg line after 2000 cycles indicates the better electrolyte diffusion into the electrode material as compared with the initial cycle. Figure 5c represents the magnified impedance spectrum of the sample for the first and 2000th cycles. The equivalent series resistance for the initial cycle is 3.2 Ω, and it becomes 2.9 Ω after 2000 cycles which clearly shows lower resistive nature of the material after cycling. Furthermore, the appearance of the small semicircle after 2000 cycles clearly indicates a very low charge transfer resistance at the electrode/electrolyte interface than the initial cycle. The lower resistance of the sample after cycling is because of better wettability, which facilitates the better electrolyte diffusion and charge transfer.

All the electrochemical results, namely the high capacitance value, high cyclability, and rate capability of the $Co_{0.85}Se$ HNWs imply that it is worth making a full-cell assembly of the $Co_{0.85}Se$ nanowire array electrode in an asymmetric configuration. An asymmetric supercapacitor has the distinct advantage of increasing the energy density of the supercapacitor by increasing the operating potential window.[28,29] It basically increases the overpotential for the water splitting so that supercapacitor works at voltages more than 1.23 V even in an aqueous medium. As $Co_{0.85}Se$ was evaluated as good cathode material, an asymmetric supercapacitor was fabricated using $Co_{0.85}Se$ as cathode and activated carbon as the anode material. All the detailed electrochemical characterizations of the activated carbon (AC) are shown in Figure SI-4 (Supporting Information). The capacitance of the activated carbon is 165 F g^{1-} for the applied current density of 1 A g^{1-}. Figure 6a is the cyclic voltammetry diagram for the activated carbon and $Co_{0.85}Se$ HNWs with their corresponding potential windows. $Co_{0.85}Se$ shows the faradic pseudocapacitance behavior as discussed before, whereas the contribution from activated carbon is totally an EDLC kind of charge storage, with a typical EDLC type rectangular nature of the curve. Within their respective potential windows, both the AC and $Co_{0.85}Se$ exhibit a stable charge storage performance. From the CV curve, the expected operating potential window of the asymmetric supercapacitor can be 1.6 V. Mass balance was done for both electrodes according to their corresponding capacitances using the following equation.[28]

$$\frac{m_{Co0.85Se}}{m_{AC}} = \frac{C_{AC}}{C_{Co0.85Se}}$$

where m is the mass of the electrode, C is the capacitance. For 1.35 mg of $Co_{0.85}Se$ (per cm^2), 5.562 mg of activated carbon was used, and it was coated on the 1 cm^2 area of CFP.

Figure 6b is the CV of the asymmetric supercapacitor with $Co_{0.85}Se$//AC at different scan rates in the 3 M KOH solution. Strong redox peaks are observed because of the pseudocapacitive nature of the $Co_{0.85}Se$ nanowire electrode. The cell voltage of the asymmetric supercapacitor is 1.6 V. The charge−discharge performance was also evaluated for the asymmetric supercapacitor up to 1.6 V for the applied current densities from 1 to 15 mA cm^{-2} (Figure 6c). The charge−discharge experiments were also performed for different voltages over a range of 1−1.6 V (Figure SI-5a, Supporting Information). It is worth noticing that with increasing cell voltage the capacitance value is also increased. After increasing the voltage from 1 to 1.6 V, the capacitance value increases by 600%, which shows a major improvement of the supercapacitor performance at higher potential (Figure SI-5b, Supporting Information). Higher operating potential has advantages of increasing the energy density of the supercapacitor according to the equation $E = {}^1/_2CV^2$. Also for a high operating potential supercapacitor, one requires fewer cells in a series connection to achieve the required desired voltage, which is very important for practical

applications. However, operating potential was restricted up to 1.6 V because water splitting takes place for more than 1.6 V.

The asymmetric supercapacitor exhibited the capacitance of 0.330 F cm^{-2} for the applied current density of 1 mA cm^{-2} (applied current density value includes the area of both $Co_{0.85}Se$ and activated carbon). This value is clearly better than the previous reports on SnSe nanosheet or $GaSe_2$ based nanostructures.[13,14] As for the single electrode performance of $Co_{0.85}Se$ HNWs, very high rate performance was also observed for full-cell configuration. It was found that more than 70% of the capacitance retention takes place even upon application of 15 times higher current density, which indicates the high rate capability of the asymmetric supercapacitor (Figure 6d).

Cyclic stability was also performed for this asymmetric supercapacitor up to 1000 cycles in the same medium with the applied current density of 5 mA cm^{-2}. A highly stable performance was witnessed with more than 94% of capacitance retention after 1000 cycles (Figure 7a). The cyclability result clearly reveals the high performance of the $Co_{0.85}Se$ HNWs in full-cell asymmetric supercapacitor configuration. The energy densities of the asymmetric supercapacitor were also calculated for different applied current densities (Figure 7b). The maximum energy density obtained is 6×10^{-5} Wh cm^{-2} which is comparable with that of the $NiO@MnO_2$ hybrid nanostructure[30] and better than carbon based materials.[31,32]

The performance of the $Co_{0.85}Se$ HNW-based electrode is quite good for single-electrode-based performance. The option of making hybrid materials using $Co_{0.85}Se$ can be explored in the future to enhance the areal capacitance and energy density. Further $Co_{0.85}Se$ can be grown on several flexible conductive materials for making a flexible gel-based solid-state supercapacitor.

4. CONCLUSION

A $Co_{0.85}Se$ hollow nanowire (HNW) array with dense self-organized morphology is synthesized by wet chemical hydrothermal selenization of initially grown cobalt hydroxyl carbonate nanowires on conductive carbon fiber paper. It exhibits an impressive areal capacitance values of 929.5 mF cm^{-2} (at 1 mA cm^{-2}) and 600 mF cm^{-2} (at 15 mA cm^{-2}, 60% retention). On the basis of the mass loading determination, this corresponds to a very high gravimetric capacitance of 674 Fg^{1-} (for 2 mA cm^{-2} or 1.48 Ag^{1-}) and 444 Fg^{1-} (for 15 mA cm^{-2} or 11 Ag^{1-}). The full-cell asymmetric configuration with the $Co_{0.85}Se$ HNWs as cathode and activated carbon as anode also shows promising results.

■ ASSOCIATED CONTENT

Supporting Information

The relation between the peak current versus the square root of scan rate; conductivity and gravimetric capacitance of the $Co_{0.85}Se$ nanowire; *CV*, charge−discharge, and gravimetric capacitance of the activated carbon at different current densities; and potential dependence of charge−discharge and areal capacitance of asymmetric supercapacitor. This material is available free of charge via the Internet at http://pubs.acs.org.

■ AUTHOR INFORMATION

Corresponding Authors

*E-mail: abhikchm@gmail.com.
*E-mail: sb.ogale@ncl.res.in.

Author Contributions

The manuscript was written through contributions of all authors. All authors have given approval to the final version of the manuscript

Notes

The authors declare no competing financial interest.

■ ACKNOWLEDGMENTS

The authors would like to thank the Council of Scientific and Industrial Research (CSIR) for funding under the TAP-SUN program.

■ REFERENCES

(1) Simon, P.; Gogotsi, Y. Materials for Electrochemical Capacitors. *Nat. Mater.* **2008**, *7*, 845−854.
(2) Dunn, B.; Kamath, H.; Tarascon, J. Electrical Energy Storage for the Grid: A Battery of Choices. *Science* **2011**, *334*, 928−935.
(3) Zhoua, Z.; Benbouzida, M.; Charpentierb, J. F.; Scuillerb, F.; Tang, T. A Review of Energy Storage Technologies for Marine Current Energy Systems. *Renewable Sustainable Energy Rev.* **2013**, *18*, 390−400.
(4) Zhang, L. L.; Zhao, X. S. Carbon-Based Materials as Supercapacitor Electrodes. *Chem. Soc. Rev.* **2009**, *38*, 2520−2531.
(5) Lu, Q.; Chen, J. G.; Xiao, J. Q. Nanostructured Electrodes for High-Performance Pseudocapacitors. *Angew. Chem., Int. Ed.* **2013**, *52*, 1882−1889.
(6) Augustyn, V.; Simon, P.; Dunn, B. Pseudocapacitive Oxide Materials for High-Rate Electrochemical Energy Storage. *Energy Environ. Sci.* **2014**, *7*, 1597−1614.
(7) Xu, Y.; Huang, X.; Lin, Z.; Zhong, X.; Huang, Y.; Duan, X. One-Step Strategy to Graphene/$Ni(OH)_2$ Composite Hydrogels as Advanced Three-Dimensional Supercapacitor Electrode Materials. *J. Nano Res.* **2013**, *6*, 65−76.
(8) Kang, J.; Hirata, A.; Kang, L.; Zhang, X.; Hou, Y.; Chen, L.; Li, C.; Fujita, T.; Akagi, K.; Chen, M. Enhanced Supercapacitor Performance of MnO_2 by Atomic Doping. *Angew. Chem., Int. Ed.* **2013**, *125*, 1708−1711.
(9) Zhang, G.; Lou, X. W. General Solution Growth of Mesoporous $NiCo_2O_4$ Nanosheets on Various Conductive Substrates as High-Performance Electrodes for Supercapacitors. *Adv. Mater.* **2013**, *25*, 976−979.
(10) Xiao, J.; Wan, L.; Yang, S.; Xiao, F.; Wang, S. Design Hierarchical Electrodes with Highly Conductive $NiCo_2S_4$ Nanotube Arrays Grown on Carbon Fiber Paper for High-Performance Pseudocapacitors. *Nano Lett.* **2014**, *14*, 831−838.
(11) Jiang, Z.; Lu, W.; Li, Z.; Ho, K. H.; Li, X.; Jiao, X.; Chen, D. Synthesis of Amorphous Cobalt Sulfide Polyhedral Nanocages for High Performance Supercapacitors. *J. Mater. Chem. A* **2014**, *2*, 8603−8606.
(12) Luoa, F.; Lia, J.; Yuanb, H.; Xiao, D. Rapid Synthesis of Three-Dimensional Flower-Like Cobalt Sulfide Hierarchitectures by Microwave Assisted Heating Method for High-Performance Supercapacitors. *Electrochim. Acta* **2014**, *123*, 183−189.
(13) Wei, W.; Mi, L.; Gao, Y.; Zheng, Z.; Chen, W.; Guan, X. Partial Ion-Exchange of Nickel-Sulfide-Derived Electrodes for High Performance Supercapacitors. *Chem. Mater.* **2014**, *26* (11), 3418−3426.
(14) Zhang, H.; Yu, X.; Guo, D.; Qu, B.; Zhang, M.; Li, Q.; Wang, T. Synthesis of Bacteria Promoted Reduced Graphene Oxide-Nickel Sulfide Networks for Advanced Supercapacitors. *ACS Appl. Mater. Interfaces* **2013**, *5*, 7335−7340.
(15) Chen, H.; Jiang, J.; Zhang, L.; Wan, H.; Qi, T.; Xia, D. Highly Conductive $NiCo_2S_4$ Urchin-Like Nanostructures for High-Rate Pseudocapacitors. *Nanoscale* **2013**, *5*, 8879−8883.
(16) Zhang, C.; Yin, H.; Han, M.; Dai, Z.; Pang, H.; Zheng, Y.; Lan, Y. Q.; Bao, J.; Zhu, J. Two-Dimensional Tin Selenide Nanostructures for Flexible All-Solid-State Supercapacitors. *ACS Nano* **2014**, *8*, 3761−3770.

(17) Wang, X.; Liu, B.; Wang, Q.; Song, W.; Hou, X.; Chen, D.; Cheng, Y. B.; Shen, G. Three-Dimensional Hierarchical $GeSe_2$ Nanostructures for High Performance Flexible All-Solid-State Supercapacitors. *Adv. Mater.* **2013**, *25*, 1479−1486.
(18) Zhang, L. F.; Zhang, C. Y. Multifunctional $Co_{0.85}Se$/Graphene Hybrid Nanosheets: Controlled Synthesis and Enhanced Performances for the Oxygen Reduction Reaction and Decomposition of Hydrazine Hydrate. *Nanoscale* **2014**, *6*, 1782−1789.
(19) Gong, F.; Wang, H.; Xu, X.; Zhou, G.; Wang, Z. S. In Situ Growth of Co(0.85)Se and Ni(0.85)Se on Conductive Substrates as High-Performance Counter Electrodes for Dye-Sensitized Solar Cells. *J. Am. Chem. Soc.* **2012**, *134* (26), 10953−10958.
(20) Yang, L.; Cheng, S.; Ding, Y.; Zhu, X.; Wang, Z. L.; Liu, M. Hierarchical Network Architectures of Carbon Fiber Paper Supported Cobalt Oxide Nanonet for High-Capacity Pseudocapacitors. *Nano Lett.* **2012**, *12*, 321−325.
(21) Huang, X. H.; Zhan, Z. Y.; Wang, X.; Zhang, Z.; Xing, G. Z.; Guo, D. L.; Leusink, D. P. Rayleigh-Instability-Driven Simultaneous Morphological and Compositional Transformation from Co Nanowires to CoO Octahedral. *Appl. Phys. Lett.* **2010**, *97*, 203112.
(22) Zhang, G. Q.; Wu, H. B.; Hoster, H. E.; Park, M. B. C.; Lou, X. W. Single-Crystalline $NiCo_2O_4$ Nanoneedle Arrays Grown on Conductive Substrates as Binder-Free Electrodes for High-Performance Supercapacitors. *Energy Environ. Sci.* **2012**, *5*, 9453−9456.
(23) Kim, J. H.; Kang, S. H.; Zhu, K.; Kim, J. Y.; Neale, N. R.; Frank, A. J. Ni−NiO Core−Shell Inverse Opal Electrodes for Supercapacitors. *Chem. Commun.* **2011**, *47*, 5214−5216.
(24) Salari, M.; Aboutalebi, S. H.; Konstantinov, K.; Liu, H. K. A Highly Ordered Titania Nanotube Array as a Supercapacitor Electrode. *Phys. Chem. Chem. Phys.* **2011**, *13*, 5038−5041.
(25) Xiao, W.; Xia, H.; Fuh, J. Y. H.; Lu, L. Electrochemical Synthesis and Supercapacitive Properties of ε-MnO_2 with Porous/Nanoflaky Hierarchical Architectures. *J. Electrochem. Soc.* **2009**, *156*, A627−A633.
(26) Liu, J.; Jiang, J.; Cheng, C.; Li, H.; Zhang, J.; Gong, H.; Fan, H. J. Co_3O_4 Nanowire@MnO_2 Ultrathin Nanosheet Core/Shell Arrays: A New Class of High-Performance Pseudocapacitive Materials. *Adv. Mater.* **2011**, *23*, 2076−2081.
(27) Xu, J.; Wang, Q.; Wang, X.; Xiang, Q.; Liang, B.; Chen, D.; Shen, G. Flexible Asymmetric Supercapacitors Based upon Co_9S_8Nanorod//Co_3O_4@RuO_2 Nanosheet Arrays on Carbon Cloth. *ACS Nano* **2013**, *7*, 5453−5462.
(28) Wang, F.; Xiao, S.; Hou, Y.; Hu, C.; Liua, L.; Wu, Y. Electrode Materials for Aqueous Asymmetric Supercapacitors. *RSC Adv.* **2013**, *3*, 13059−13084.
(29) Chang, J.; Jin, M.; Yao, F.; Kim, T. H.; Le, V. T.; Yue, H.; Gunes, F.; Li, B.; Ghosh, A.; Xie, S.; Lee, Y. H. Asymmetric Supercapacitors Based on Graphene/MnO_2 Nanospheres and Graphene/MoO_3 Nanosheets with High Energy Density. *Adv. Funct. Mater.* **2013**, *23*, 5074−5083.
(30) Liu, J.; Jiang, J.; Bosmanc, M.; Fan, H. J. Three-Dimensional Tubular Arrays of MnO_2−NiO Nanoflakes With High Areal Pseudocapacitance. *J. Mater. Chem.* **2012**, *22*, 2419−2426.
(31) Du, C.; Yeh, J.; Pan, N. High Power Density Supercapacitors Using Locally Aligned Carbon Nanotube Electrodes. *Nanotechnology* **2005**, *16*, 350−353.
(32) Niu, C.; Sichel, E. K.; Hoch, R.; Moy, D.; Tennent, H. High Power Electrochemical Capacitors Based on Carbon Nanotube Electrodes. *Appl. Phys. Lett.* **1997**, *70*, 1480−1482.